

Research Paper

Performance enhancement of desiccant wheels by adsorption/desorption in stages with type-S isotherm desiccants

Zhengrong Li^{a,b}, Ruiyang Tao^{a,*}^a School of Mechanical Engineering, Tongji University, Shanghai 201800, China^b Key Laboratory of Performance Evolution and Control for Engineering Structures of Ministry of Education, Tongji University, Shanghai 200092, China

ARTICLE INFO

Keywords:

Desiccant wheel
Solid desiccants
Dehumidification
Adsorption isotherm

ABSTRACT

Desiccant wheels coated with desiccants possessing a single kind of adsorption isotherm face the drawback that the moisture transfer driving force decreases along the direction of air flow in the channel, which hinders the efficiency of regeneration and dehumidification processes. In this study, a new concept of adsorption/desorption in stages with type-S isotherm desiccants was proposed to improve the performance of a counter flow type desiccant wheel by increasing the moisture transfer driving force during both dehumidification and regeneration processes. The numerical results show that compared with conventional wheel made up of silica gel, the two desiccant wheels with various hypothetical type-S isotherm desiccants designed in this study output air with more stable humidity during dehumidification, and have superior performance when both cycling time (t_{cyc}) is high and regeneration temperature ($T_{r,i}$) exceeds the critical value.

1. Introduction

The working principle of the counter flow type desiccant wheel is shown in Fig. 1[1]. A rotating desiccant wheel composed of many small channels coated with the mix of desiccants and matrix is divided into the dehumidification part and the regeneration part. The moisture of the process air can be absorbed by desiccants during dehumidification and desorbed by hot air during regeneration. A desiccant wheel can be used to achieve independent control of air temperature and humidity, which avoids many problems of cooling dehumidification technology[2]. As the most prevailing solid dehumidification technology on the market, desiccant wheels have significant application potential in low-energy buildings, data centers, and lithium battery factories[3]. Pennington [4] first proposed a patent for a desiccant wheel in 1955, and researchers currently remain of strong interest in this field. Since the 21st century, new system design concepts of desiccant wheels, such as multi-stage [5,6], multi-partition[7], non-adiabatic multi-channel[8], and water-cooled[9] systems, have been developed successively to improve dehumidification performance and energy efficiency. Some parameter optimization methods for optimizing regeneration temperature, rotation speed, partition proportion and channel geometric parameters have also been proposed[10–13]. In addition, many innovative desiccants with high moisture uptake capacity and quick response have been synthesized, such as compound desiccants, nanoporous inorganic materials,

and polymer desiccants[14].

The adsorption isotherm of the desiccants significantly influences the final performance of the desiccant wheel, and can be divided into six types according to the definition of the International Union of Pure and Applied Chemistry (IUPAC)[3], as shown in Fig. 2. Researchers have agreed that suitable desiccant isotherm under different scenarios varies [15–19]. Novosel[18] proposed that type-1 M is the optimal isotherm for comfortable air conditioning at high regeneration temperatures. Sultan [17] concluded a similar result and further pointed out that type-III and type-V only work in a high relative humidity range despite their regeneration requiring relatively low temperatures. Feng[16] numerically simulated the performance of a desiccant wheel with various hypothetical isotherms and revealed that the type-S isotherm is not an ideal isotherm because the variation in the relative humidity of the air along the flow direction in the channels will lead to the desiccant wheel working at its worst range.

In fact, a desiccant wheel coated with a single-kind isotherm desiccants always faces the limitation of the moisture transfer driving force declining along the flow channel, which restricts the dehumidification performance and energy efficiency of the system. Sultan [17] mentioned the concept that desiccants with different isotherms can be used to remove this limitation by addressing the different stages of air flow along the channel in order. Muthu[32] numerically simulated the performance of a desiccant wheel coated with silica gel and molecular sieve, as shown in Fig. 3. Compared to the full silica gel wheel and full

* Corresponding author.

Nomenclature	
A	cross-sectional area of gas duct, m^2
A_{tot}	total cross-sectional area of a channel with adsorbent layer, m^2
C	wetted perimeter of the cross-section, m
D_G	gas diffusivity, m^2/s
D_O	ordinary molecular diffusivity, m^2/s
D_K	Knudsen diffusivity, m^2/s
D_S	surface diffusivity, m^2/s
D_{va}	vapor diffusivity in air, m^2/s
G	mass flow rate, kg/s
K_y	convective mass transfer coefficient, m/s
L	channel length, m
L_v	latent heat of condensation, (J/kg)
P	pressure, pa
P_{vs}	saturated vapor pressure, pa
T	temperature, K
W	adsorbate uptake, kg/kg
Y	humidity ratio (kg moisture/ kg dry air)
a	channel height, mm
b	channel base, mm
c_p	specific heat, $\text{J}/(\text{kg K})$
f	structural void fraction, A/A_{tot}
h	Specific enthalpy, J/kg
k	thermal conductivity, $\text{W}/(\text{m K})$
t	time, s
u	velocity, m/s
Nu	Nusselt number
Sh	Sherwood number
RH	relative humidity
MRR	moisture removal rate, kg/s
M_1	molecular weight of water (kg/mol)
$DCOP$	dehumidification coefficient of performance
Greek symbols	
ε	adsorbent porosity
ν_r	porous radius, mm
δ	adsorbent thickness, m
ϕ	mass fraction of active material in adsorbent coating
α	convective heat transfer coefficient, m/s
τ	tortuosity
ρ	density, kg/m^3
Subscripts	
a	dry air
d	dry desiccant
g	gas stream
i	initial state
l	liquid water
m	matrix
p	process air
r	regeneration air
v	water vapor
eq	equilibrium state
sg	silica gel
wd	wetted desiccant
atm	atmospheric

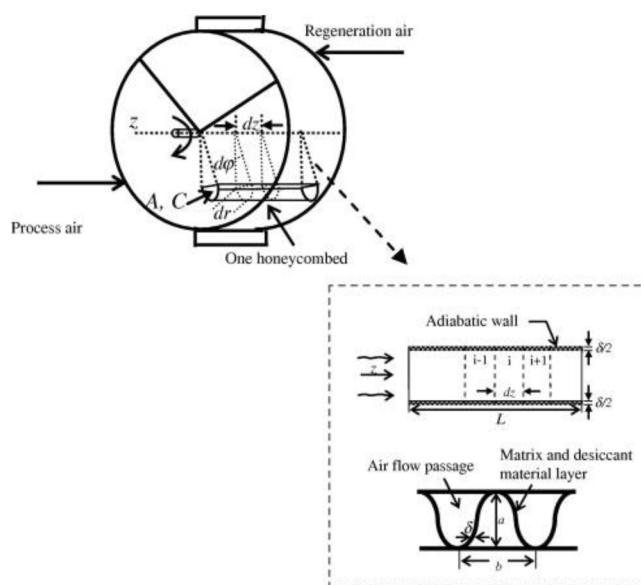


Fig. 1. The working principle and the computational domain of a counter flow type desiccant wheel.

molecular sieve wheel, this so-called hybrid desiccant wheel showed a limited performance advantage because this silica gel/molecular hybrid configuration failed to increase the moisture transfer driving force during regeneration.

This study proposed a new concept of adsorption/desorption in stages with type-S isotherm desiccants to improve the performance of a counter flow type desiccant wheel by increasing the moisture transfer

driving force during both dehumidification and regeneration processes (Table 1 categories the commercially available Type-S isotherms desiccants according to the step rise in different RH range). Fig. 4 suggests an illustration for example of the staged adsorption/desorption that, a type-S isotherm desiccant with a step rise in the high humidity range (so-called hydrophobic desiccant) can be used to preprocess the high humidity airflow, and the desiccant with a step rise in the middle humidity range (so-called moderate desiccant) dehumidifies the airflow in the second stage. Finally, the desiccant with a step rise in the extremely low humidity range (so-called hydrophilic desiccant) is used to conduct deep dehumidification of the airflow. With the help of type-S isotherm desiccants, the moisture transfer driving force declining along the air flow channel problem can be solved simultaneously in the dehumidification and regeneration stages of counterflow-type desiccant wheels.

To clarify the performance improvement effect of the desiccant wheel that may be brought by adsorption/desorption in stages with type-S isotherm desiccants and to preliminarily understand its system operation characteristics, two different hybrid configurations named S1 and S2 with hypothetical desiccants were considered, as presented in Table 2. A mathematical model was established to carry out the performance comparison study between the hybrid desiccant wheels S1/S2 and a full silica gel wheel.

2. Mathematical model

Mathematical models of desiccant wheels can be classified into two main categories: (1) gas-side resistance (GSR) model and (2) gas and solid-side resistance (GSSR) model which can be further subdivided into pseudo-gas-side (PGS) model, gas and solid-side (GSS) model and parabolic concentration profile (PCP) model [33,34]. In this study, the GSS mathematical model established by Ge [1] with slight changes was used to simulate the periodic transient of the counterflow-type desiccant wheel.

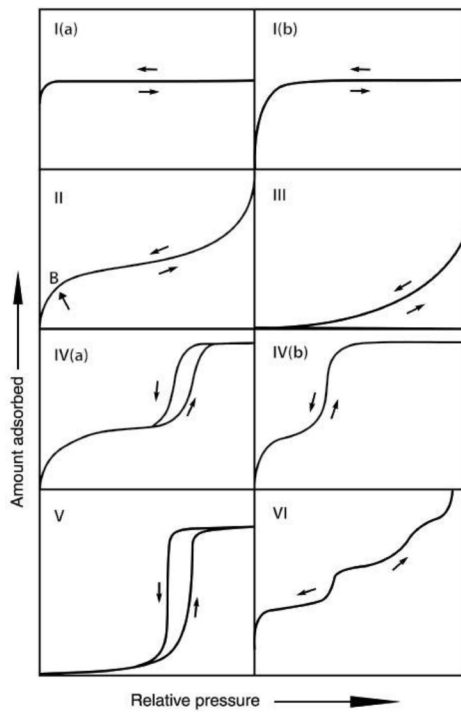


Fig. 2. Classification of the adsorption isotherms according to IUPAC.

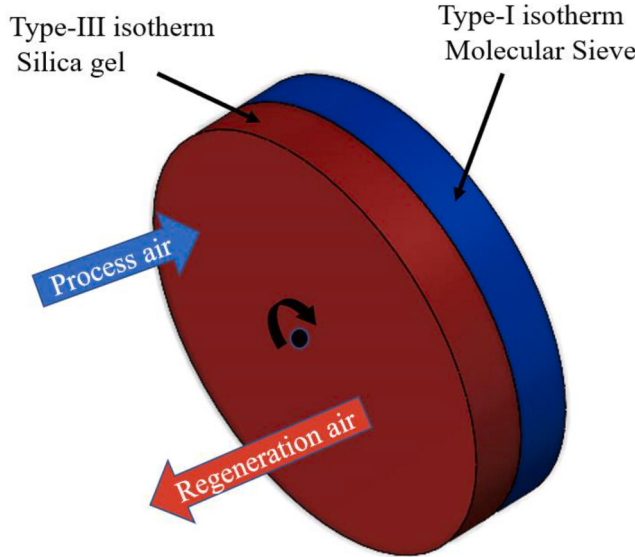


Fig. 3. Schematic of the hybrid desiccant wheel with Silica gel and Molecular Sieve.

2.1. Basic assumptions and governing equations

Basic Assumptions:

- 1) The temperature and moisture content gradients in the circumferential and radial directions are negligible.
- 2) Heat conduction in humid air and the matrix is negligible.
- 3) Sh was assumed to be equal to Nu based on the analogy between mass and heat transfer [35] and be constant over the entire dehumidifier.
- 4) All honeycombed channels that make up the rotary desiccant wheel are identical.

Table 1
Example of the commercially available S-type isotherm desiccants.

Category	Hydrophilic	Moderate	Hydrophobic
Step rise	0–0.3 RH SAPO-18[20]	0.3–0.5 RH AQSOA-205[21]	0.5–1 RH FSM-16 [22]
	TAPSO-34[20]	MIL-101(Cr)[23]	MCM-41[24]
Name	AQSOA-Z01[21]	Activated carbon [25]	MCM-48[24]
	AQSOA-Z02[21]	Carbon-based aerogel	SBA-15[24]
		A-41[26]	
		MOF-801(Zr)[27]	Carbon-based aerogel
		NU-1500 [28]	A-54[26]
		MIL-125(Ti)-NH2[29]	SiGe10-40[31]
		CAU-10-H[21]	MOF-841[30]
			SiO ₂ aerogel[31]
			UiO-66(Zr)[30]

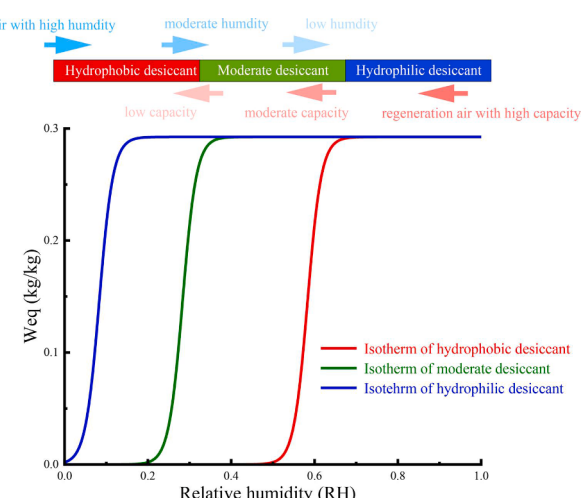


Fig. 4. Illustration of the adsorption/desorption in stages using desiccants with hypothetical S-type isotherm.

Table 2

Hybrid desiccant wheel configurations studied.

Hybrid configuration S1	Hybrid configuration S2
Isotherm equation form:	
$W_{eq} = \frac{W_{max}}{1 + e^{-B \cdot RH + C}}$, $W_{max} = 0.2925 \text{ kg/kg}$	
Left: 1/2 Desiccant 1, B = 50, C = 20	Left: 1/3 Desiccant 4, B = 60, C = 35
Right: 1/2 Desiccant 2, B = 50, C = 5	Middle: 1/3 Desiccant 5, B = 60, C = 17
	Right: 1/3 Desiccant 6, B = 60, C = 5

- 5) Matrix material and desiccant material are evenly distributed in the layer.
- 6) The hygroscopic capacity of the matrix material is negligible compared to that of the adsorbent.
- 7) The inlet air conditions are uniform in space but may vary with time.
- 8) The thermophysical properties of the dry desiccant material as well as of the matrix are constant.
- 9) The vapor enters the pores, diffuses in the pores, and meanwhile is adsorbed. The heat of adsorption is set free in the desiccant layer immediately when water vapor enters the porous layer.
- 10) The pressure loss of the air stream in the axial direction is negligible. It is, of course, relevant to calculate the fan power, but it is less relevant for discussion of the heat and mass transfer processes.
- 11) The thermophysical, thermodynamic and fundamental adsorption properties, including the saturation adsorption capacity, of the hypothetical desiccants were considered as the same as those of silica gel to highlight the significance of the isotherm shape and simplicity of analysis.

The governing equations were derived based on the conservation of moisture and conservation of energy for the air and solid side.

Moisture conservation on the air side:

$$\rho_a f A_{tot} \left(\frac{\partial Y_a}{\partial t} + u \frac{\partial Y_a}{\partial z} \right) = K_y C (\rho_a Y_d - \rho_a Y_a) \quad (1)$$

Moisture conservation on the solid side

$$\begin{aligned} & \rho_a \varepsilon (1-f) A_{tot} \frac{\partial Y_d}{\partial t} + \rho_d (1-\varepsilon) (1-f) A_{tot} \phi \frac{\partial W}{\partial t} \\ &= \rho_a \varepsilon (1-f) A_{tot} D_G \frac{\partial^2 Y_d}{\partial z^2} + \rho_d (1-\varepsilon) (1-f) A_{tot} \phi D_S \frac{\partial^2 W}{\partial z^2} + K_y \rho_a C (Y_a - Y_d) \end{aligned} \quad (2)$$

Energy conservation on the gas side:

$$\rho_g c_{pg} f A_{tot} \left(\frac{\partial T_a}{\partial t} + u \frac{\partial T_a}{\partial z} \right) = \alpha C (T_d - T_a) + K_y c_{pv} C (\rho_a Y_d - \rho_a Y_a) (T_d - T_a) \quad (3)$$

the $\rho_g = \rho_a (1 + Y_a)$, $c_{pg} = c_{pa} + Y_a c_{pv}$, are respectively the density and heat capacity of the moist air.

Energy conservation on the solid side:

$$\begin{aligned} & \rho_m c_{pm} (1-f) A_{tot} (1-\varepsilon) (1-\phi) \frac{\partial T_d}{\partial t} + \rho_d c_{pwd} (1-f) A_{tot} (1-\varepsilon) \phi \left(\frac{\partial T_d}{\partial t} - \frac{k_{wd}}{c_{pwd} \rho_d} \frac{\partial^2 T_d}{\partial z^2} \right) \\ &= \alpha C (T_a - T_d) + K_y \rho_a c_{pv} C (Y_a - Y_d) (T_a - T_d) + \rho_d (1-\varepsilon) (1-f) A_{tot} \phi \frac{\partial W}{\partial t} Q_{st} \end{aligned} \quad (4)$$

where a simplified calculation, $k_{wd} = (1 - \varepsilon) k_d + \varepsilon k_l$, represents the heat conductivity of the wetted desiccant. The $c_{pwd} = c_{pd} + c_{pl} W$ is the specific heat of the wetted desiccant.

Table 3

Properties of the air, desiccants and the channel.

Common Input data			
c_{pv}	1872 J/(kg K)	k_y	0.0196 W/(m K)
c_{pa}	1007 J/(kg K)	k_a	0.0263 W/(m K)
c_{pm}	880 J/(kg K)	k_l	0.613 W/(m K)
c_{pl}	4180 J/(kg K)	k_{sg}	0.011 W/(m K)
c_{psg}	1340 J/(kg K)	ν_r	$5.0 \times 10^{-7} \text{ m}$
ρ_m	625 kg/m ³	ε	0.3
ρ_{sg}	930 kg/m ³	ϕ	0.8
ρ_a	1.1614 kg/m ³	τ	3.0

Channel geometry

sigmoid channel: $a = 1.5 \text{ mm}$ $b = 3 \text{ mm}$ $\delta = 0.25 \text{ mm}$ $L = 0.2 \text{ m}$

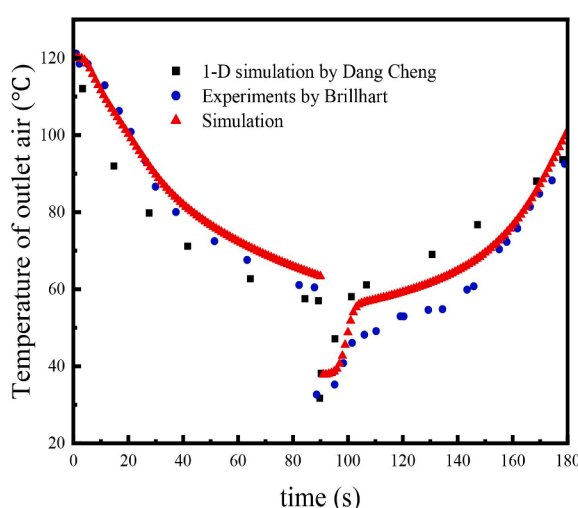
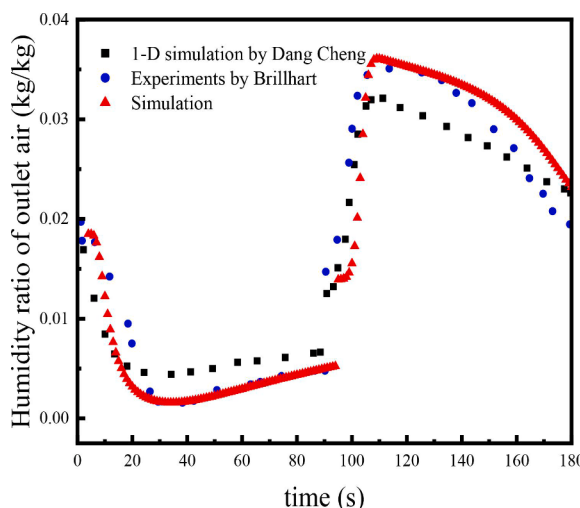


Fig. 5. Model validation by comparing the air conditions of outlet air (0 ~ 90 s dehumidification, 90 ~ 180 s regeneration).

2.2. Initial and boundary conditions

Boundary conditions:

$$\begin{aligned} T_a(0, t) &= T_{p,i} \text{ for process air} \\ T_a(z, t) &= T_{r,i} \text{ for regeneration air} \\ Y_a(0, t) &= Y_{p,i} \text{ for process air} \\ Y_a(z, t) &= Y_{r,i} \text{ for regeneration air} \end{aligned}$$

Initial conditions:

$$\begin{aligned} T_a(z, 0) &= T_d(z, 0) = T_{p,i} \\ Y_a(z, 0) &= Y_d(z, 0) = Y_{p,i} \\ W(z, 0) &= W_{eq}(T_{p,i}, Y_{p,i}) \end{aligned} \quad (6)$$

It was assumed that the entrance and existence of each channel on the solid side have an adiabatic impermeable boundary. This corresponds to neglecting the diffusive terms in the axial direction, which results in:

$$\begin{aligned} \frac{\partial T_d}{\partial z} \Big|_{z=0} &= \frac{\partial T_d}{\partial z} \Big|_{z=L} = 0 \\ \frac{\partial Y_d}{\partial z} \Big|_{z=0} &= \frac{\partial Y_d}{\partial z} \Big|_{z=L} = 0 \end{aligned} \quad (7)$$

2.3. Auxiliary conditions

The Clapeyron equation describes the relationship between the absolute humidity and relative humidity:

$$Y = \frac{0.62188RH}{P_{atm}/P_{vs} - RH} \quad (8)$$

$$P_{vs} = \exp[23.196 - 3816.44/(T - 46.13)] \quad (9)$$

Both gas diffusion and surface diffusion happen inside the desiccant layer. The gas diffusion is a combination of Knudsen diffusion and ordinary molecular diffusion [36]:

$$\begin{aligned} D_G &= \frac{1}{\tau} \left(\frac{1}{D_O} + \frac{1}{D_K} \right)^{-1} \\ D_O &= 1.735 \times 10^{-9} \frac{T_d^{1.685}}{P/P_{atm}} \\ D_K &= 97\nu_r \left(\frac{T_d}{M_1} \right)^{0.5}, M_1 = 0.018 \text{ kg/mol} \end{aligned} \quad (10)$$

Surface diffusivity can be calculated as follow [37]:

$$\begin{aligned} D_S &= \frac{1}{\tau} D_0 \exp \left(-0.974 \times 10^{-3} \frac{Q_{st}}{T} \right) \\ D_0 &= 1.6 \times 10^{-6} \text{ m}^2/\text{s} \end{aligned} \quad (11)$$

The isotherm and adsorption heat of silica gel are given by [38]:

$$Q_{st} = \begin{cases} -13400W + 3500, & W \leq 0.05 \\ -1400W + 2950, & W > 0.05 \end{cases} \quad (12)$$

$$RH = (3.4188W_{eq})^{1.3369} \quad (13)$$

The cross-sectional areas, the wet perimeter, and the structural void fraction of the channel were estimated as follows:

$$A = ab \sqrt{\frac{1}{2}}$$

$$A_{tot} = \frac{1}{2} \times [b + \delta\sqrt{2}] \times [a + \delta\sqrt{2}] \quad (14)$$

$$C \approx b + \sqrt{b^2 + (a\pi)^2} \frac{3 + (\frac{2b}{a\pi})^2}{4 + (\frac{2b}{a\pi})^2}$$

$$f = A / A_{tot}$$

In addition, the following heat and mass transfer relations were adopted:

$$Nu = Sh = 2.12 \quad (15)$$

$$\alpha = \frac{Nu k_a C}{4A} \quad (16)$$

$$\begin{aligned} K_y &= \frac{Sh D_{va} C}{4A}, D_{va} = 2.302 \times 10^{-5} \frac{P_0}{P} \left(\frac{T}{T_0} \right)^{1.81} \\ P_0 &= 0.98 \times 10^5 \text{ Pa}, T_0 = 256 \text{ K} \end{aligned} \quad (17)$$

Table 4
Operating conditions.

	Based Value <i>cool&humid</i>	Range	Interval
$T_{p,i}$ (°C)	20	30	
$Y_{p,i}$ (g/kg)	12.34(85 %RH)	22.89(85 %RH)	
$T_{r,i}$ (°C)	80	40–130	10
$Y_{r,i}$ (g/kg)	12.34	22.89	
u (m/s)	2		
t_{cyc} (s/r)	180	40–960	unfixed
t_p / t_{cyc}	0.5	0.2–0.8	0.1

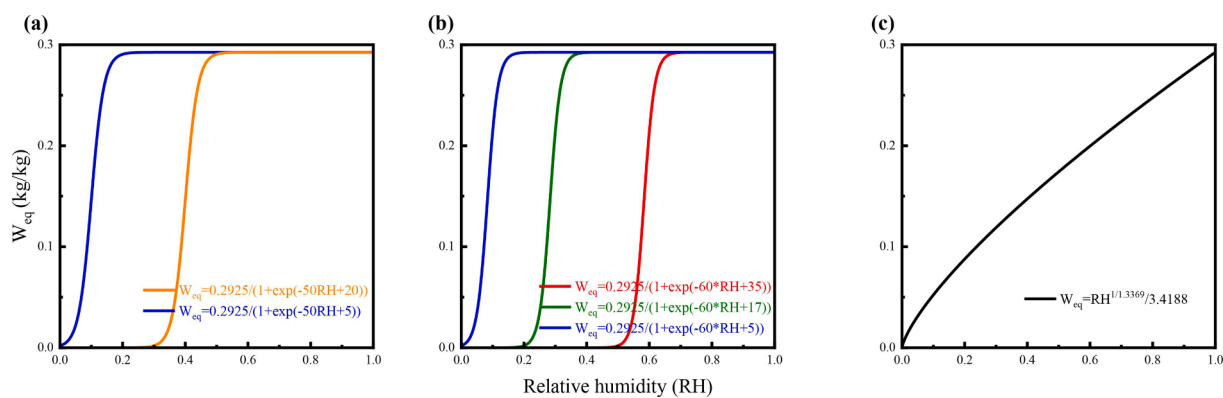


Fig. 6. The isotherms for (a) desiccants 1&2 in S1, (b) desiccants 3&4&5 in S2, and (c) silica gel.

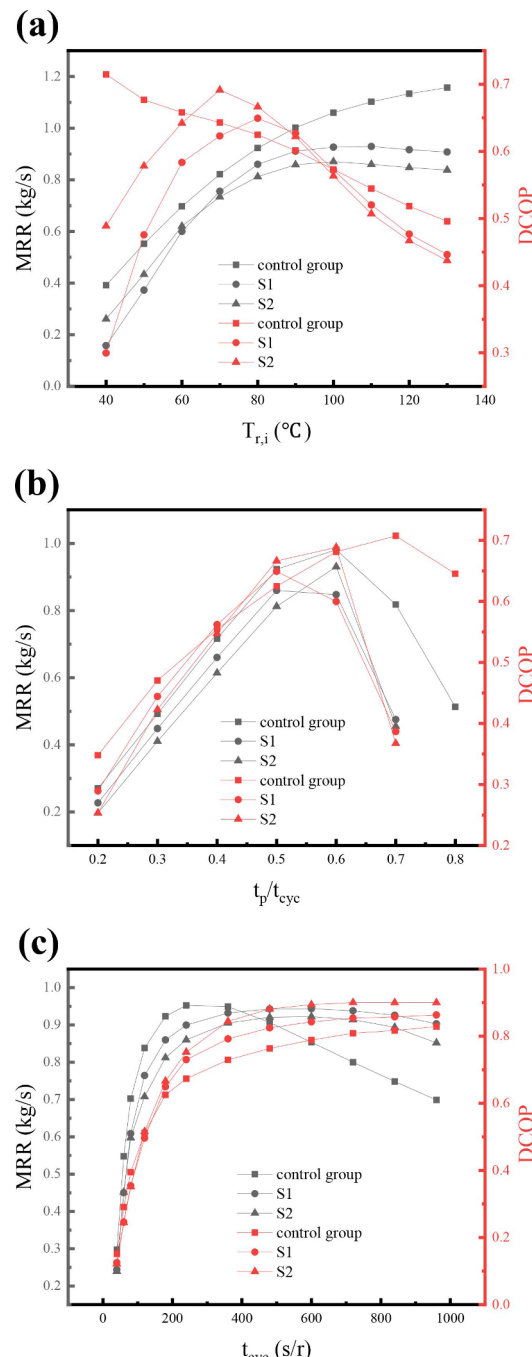


Fig. 7. Single factor performance comparison under cool&humid condition.

2.4. Solution method and model validation

Governing equations were discretized into a fully implicit finite difference scheme. An object-oriented programming language, C++, on a personal computer was adopted to solve the mathematical model with the Gauss Seidel iterative method. Considering both the time consumption and accuracy, the space step size is 1/3 cm, and the Courant number (CFL) equals 1.

The present simulated results of the silica gel wheel were validated with the simulated results of Cheng [38] and with the experimental results of Brillhart [39] as referred by Cheng as per the corresponding wheel parameters and operating conditions, as shown in Fig. 5.

3. Performance comparison between the hybrid desiccant wheel and silica gel wheel

3.1. Performance indices

In this paper, two indices (including the $DCOP$ (dehumidification coefficient of performance), the MRR (moisture removal rate)) are defined to assess the dehumidification performance of the desiccant wheel. The adsorption time and desorption time are t_p and t_r respectively. Thus, the cycle time $t_{\text{cyc}} = t_p + t_r$. The mean outlet temperature and humidity for the process air and regeneration air can be calculated by the integration of the outlet values over time t :

$$\begin{aligned} \bar{T}_{p,o} &= \frac{\int_0^{t_p} T_{p,o} dt}{t_p}, \bar{T}_{r,o} = \frac{\int_{t_p}^{t_{\text{cyc}}} T_{r,o} dt}{t_r} \\ \bar{Y}_{p,o} &= \frac{\int_0^{t_p} Y_{p,o} dt}{t_p}, \bar{Y}_{r,o} = \frac{\int_{t_p}^{t_{\text{cyc}}} Y_{r,o} dt}{t_r} \end{aligned} \quad (18)$$

For a dehumidification system, the dehumidification coefficient of performance ($DCOP$) is defined as the effective dehumidification energy (the latent heat change of the process air from the inlet state to the outlet state) divided by the enthalpy change of the regeneration air. The parameter synthetically reflects the dehumidification performance and energy consumption and can be expressed by:

$$DCOP = \frac{G_p L_v (Y_{p,i} - \bar{Y}_{p,o})}{G_r (h_{r,i} - \bar{h}_{r,o})} \quad (19)$$

where G_p is the mass flow rate of the process air stream, G_r is the mass flow rate of the regeneration air stream, and L_v is latent heat of water vapor. The diameter of the wheel was set as 0.4 m to calculate G_p and G_r .

The moisture removal rate (MRR) reflects the dehumidification capacity directly and is expressed by:

$$MRR = G_p (Y_{p,i} - \bar{Y}_{p,o}) \quad (20)$$

3.2. Simulation input

The detailed input properties of the air, the desiccants, and the channel geometry were calculated and used in the simulation as per Cheng et al. [38], and listed in Table 3. Fig. 6 gives the comparison of the isotherms between silica gel and the hypothetical desiccants investigated in this paper.

The performance of a desiccant wheel is influenced by many variable factors. This study considered regeneration temperature, cycle time and dehumidification partition proportion (defined as the ratio of the cross-sectional area of dehumidification part to the whole part of the wheel, and can be calculated as t_p/t_{cyc}) as the single factors, selecting 0.2 m as the thickness of the wheel. The performance of the desiccant wheel was investigated under two process airflow conditions: "cool&humid" and "hot&humid". The humidity ratio of regeneration air is equal to the humidity ratio of the process air based on the assumption that the regeneration air is actually the indoor return air heated by the heat source. A single-factor comparison simulation study between the two hybrid desiccant wheels and silica gel wheel was carried out under the same operating and structural parameters according to Table 4 (the unmentioned operation conditions in chapter 3 remained the based value).

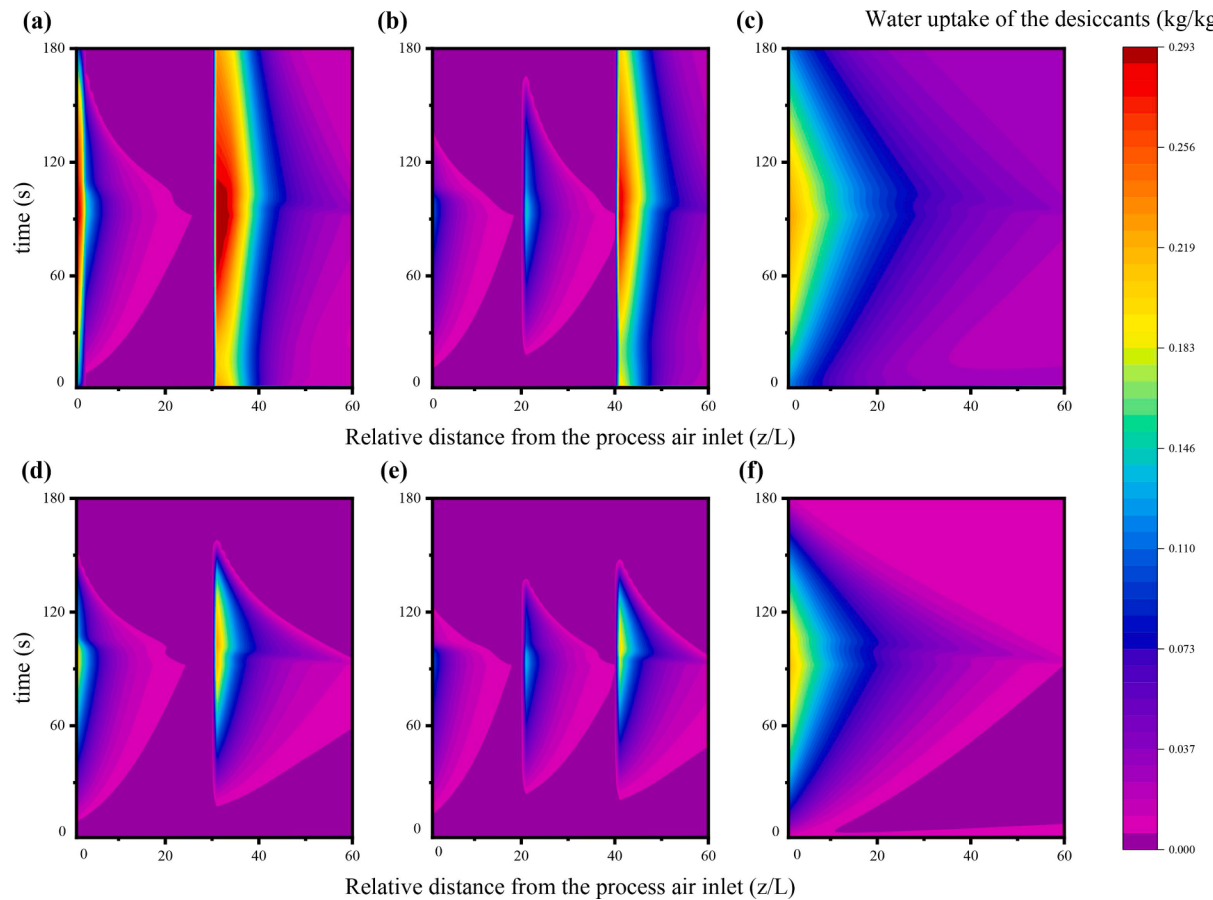


Fig. 8. Water uptake contour of the desiccants at 80 °C: (a), (b), and (c), and 130 °C: (d), (e), and (f) (0–90 s dehumidification, 90–180 s regeneration).

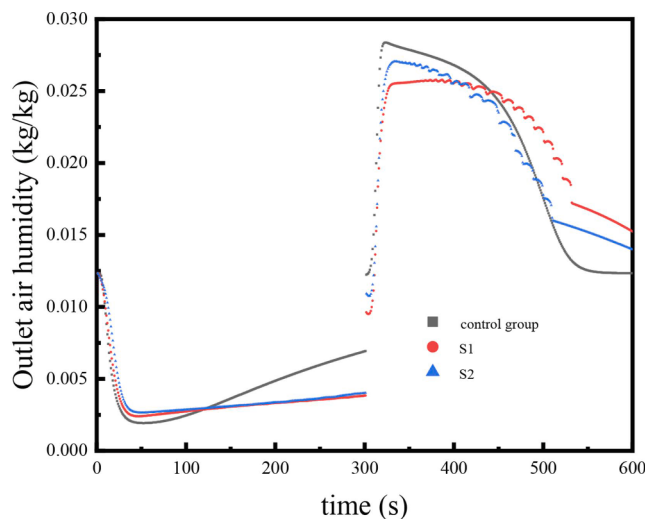


Fig. 9. Outlet air humidity change under 600 s cycling time (cool&humid) (0–300 s dehumidification, 300–600 s regeneration).

4. Results and discussion

4.1. Cool&humid condition

Fig. 7 shows the calculated DCOPs and MRRs with different operation parameters under cool&humid condition. In general, the performance of S1 and S2 at many operation conditions was weaker than that of the silica gel wheel. However, it indicates that those parameters

changed the hybrid wheels and silica gel wheel in different ways, especially that the performance advantages of the hybrid wheels emerged when the cycling time was high enough.

An optimal $T_{r,i}$ of approximately 80°C can be observed for S1 and S2. The quick performance deterioration of them with the decline of $T_{r,i}$ which was different from the silica gel wheel, can be attributed to the fact that the moderate and hydrophilic desiccants cannot be regenerated by low temperature air. Moreover, the MRRs of S1 and S2 failed to keep increasing when the $T_{r,i}$ exceeded 100°C. In fact, the MRRs were decreasing due to the excessive regeneration temperature that led to the early ended desorption and lately started adsorption (Fig. 8) that both hindered the final performance. The both S1 and S2 performed worse than the silica gel wheel under various $T_{r,i}$ and the same situation appeared while the t_p/t_{cyc} differs with an approximate optimal $t_p/t_{cyc} = 0.5$ for all wheels.

As shown in Fig. 7(c), the DCOPs of S1 and S2 remained 10 % higher than that of the silica gel wheel when the cycling time varied from 480 s to 960 s. S1 and S2 had higher MRRs as the cycling time exceeded 480 s and reached more than 20 % improvement at 720 s/r compared to the silica gel wheel. This enhancement may, as Fig. 9, brought by the continuously stable humidity of airflow in the dehumidification stage of S1 and S2, while the outlet process air humidity of the silica gel wheel increased quickly. It's easy to understand this that since the most desiccants along the channel of S1 and S2 wheels left much room for water adsorption after the early ended dehumidification stage. The latter part of each staged type-S isotherm desiccant then, after the quick saturated adsorption in their former part, could co-dehumidify sequentially the process air to the low RH range in the highly efficient way if the dehumidification continues. On the other hand, although most of the silica gel did not meet the saturation either, the moisture transfer driving force between the desiccant and the process air kept declined. This

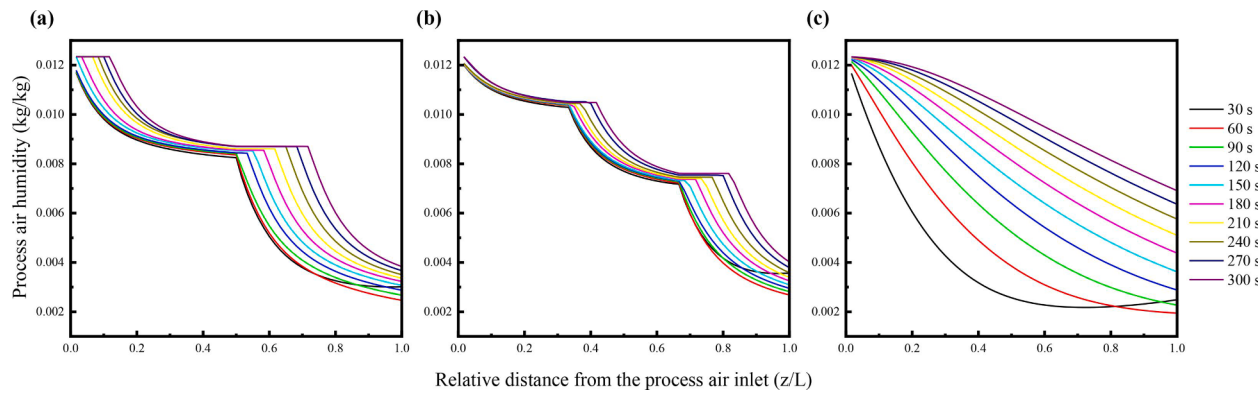


Fig. 10. The process air humidity change along the channel from 30 to 300 s.

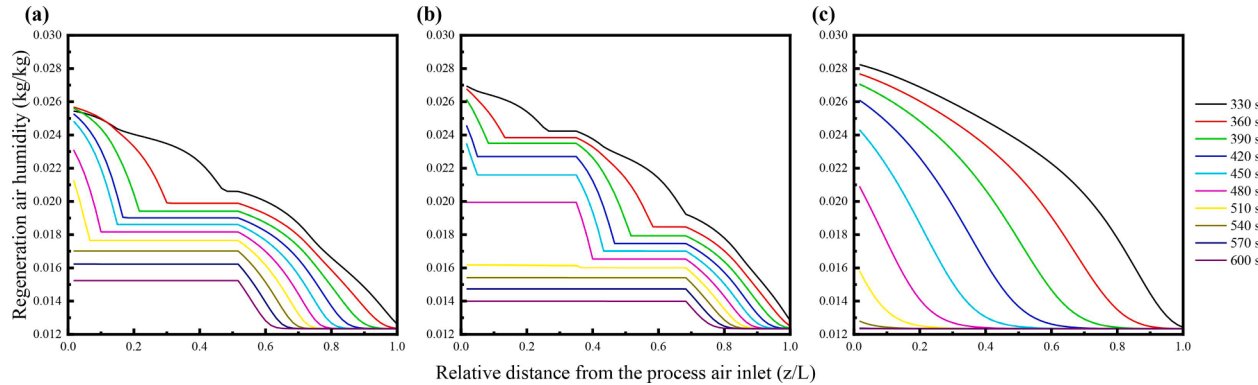


Fig. 11. The regeneration air humidity change along the channel from 330 to 600 s.

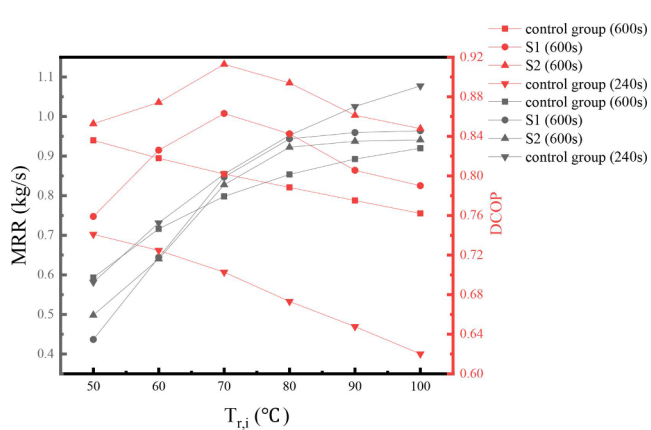


Fig. 12. Performance comparison under different regeneration temperatures (cool&humid) (S1, S2: $t_{cyc} = 600$ s; Control group: $t_{cyc} = 600$ s/ 240 s).

explanation can be verified in Fig. 10, which is a clearer comparison of how the air humidity decreased during dehumidifying.

Besides, Fig. 11 gives the proof of high regeneration efficiency of the moderate and hydrophobic desiccants in the hybrid wheels, where the water can be totally desorbed quickly (desorption completed before 540 s for the moderate desiccant in S1, before 510 s and 480 s for the moderate and hydrophobic desiccants in S2 respectively). This resulted in, as seen from Fig. 9, the rapid desorption stage (around 350 s- 500 s) of S1 and S2. Due to the less coated hydrophobic desiccant that is hard to regenerate, the S2 had shorter rapid desorption stage. The regeneration of the hydrophilic desiccants is difficult, leading to the descend of the overall desorption efficiency and implies that the hypothetical isotherm

and the coating length of the hydrophilic in this study should be optimized. In the meantime, Fig. 10 illustrates that the dehumidification of the hybrid wheels can't be as deep as the silica gel wheel at the initial stage of dehumidification. The reason behind this is the higher water uptake capacity of silica gel than the hypothesized hydrophilic desiccants in the extremely low RH range (<5%). This phenomenon explains the unsatisfactory performance of the hybrid wheels cycling in short time.

The above discussion indicates that the long cycle time is necessary for the studied hybrid wheels to perform better than the silica gel wheel. The performance of the wheels under long cycling time was further investigated. As shown in Fig. 12, when the regeneration temperature was higher than 70 °C, a slow rotation speed significantly improved the performance of the two hybrid wheels. Compared with silica gel, when the regeneration temperature varied from 70 °C-100 °C and $t_{cyc} = 600$ s, the average MRRs of S1 and S2 increased by 7.2 % and 4.8 % respectively, while the average DCOPs increased by 5.6 % and 12.4 %. The greatest performance advantages brought by the staged adsorption/desorption were at the regeneration of 80 °C, where S1 showed 10.5 % MRR and 6.9 % DCOP higher (8.1 % MRR and 13.4 % DCOP higher for S2) than the silica gel wheel. The desiccant wheels indeed should be operated with optimal cycle time, and the further comparison is important for the hybrid wheels with $t_{cyc} = 600$ s and the silica gel wheel with $t_{cyc} = 240$ s (both the optimal cycling time as shown in Fig. 7(c)). Seen in Fig. 12, the silica gel wheel exhibited superior MRRs when working at the ideal cycling time (at most 0.13 kg/s MRR higher than S2). However, the sharply decreased DCOP provides the evidence of the more efficient desorption brought by staged regeneration. Furthermore, the MRR difference between all the three wheels at 70- 80°C was small, but the hybrid wheels had remarkably amplified DCOP. It should be noted that the DCOP of S2, despite the lower MRR, was higher than that of S1, due to the earlier ended rapid desorption stage of S2 that caused

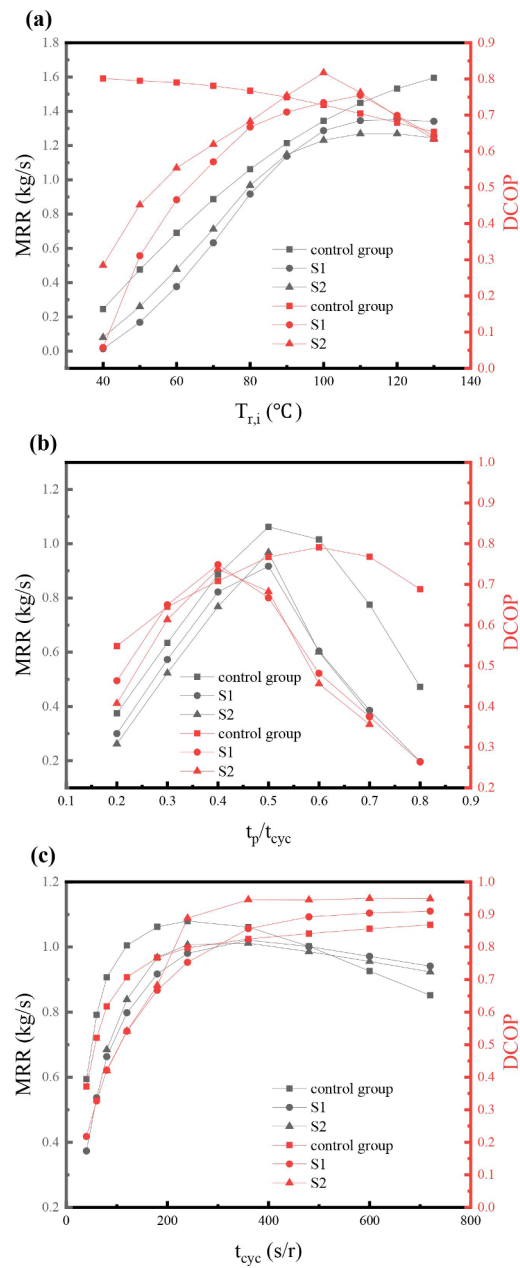


Fig. 13. Single factor performance comparison under hot&humid condition.

the higher average $T_{r,o}$.

4.2. Hot&humid condition

The performance comparison between the wheels were also investigated under hot&humid condition. It can be seen, in Fig. 13, that all three desiccant wheels had the same performance variation trend as under cool&humid condition. The optimal $T_{r,i}$ of approximately 100°C and an optimal t_p/t_{cyc} of 0.5 for the hybrid wheels were observed. Similarly, S1 and S2 did not perform better for different $T_{r,i}$ and t_p/t_{cyc} under the $t_{\text{cyc}} = 180$ s. However, they still had higher performance indices after the cycling time exceeded 480 s. The mechanism has been discussed in detail in section 2.1.

Fig. 14 shows the performance comparison between the wheels under different $T_{r,i}$ when the cycling time was 600 s. After the regeneration temperature been altered to higher than 80°C , the average MRRs of S1 and S2 increased by 19.4 % and 14.7 % respectively, while

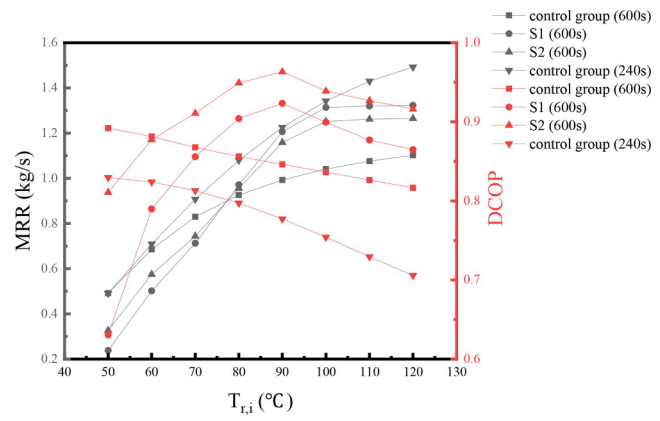


Fig. 14. Performance comparison under different regeneration temperatures (hot&humid) (S1, S2: $t_{\text{cyc}} = 600$ s; Control group: $t_{\text{cyc}} = 600$ s/ 240 s).

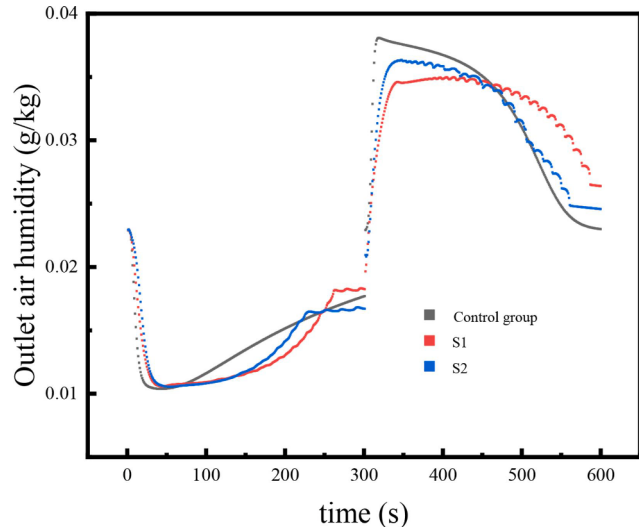


Fig. 15. Outlet air humidity change under 600 s cycling time (hot&humid) (0–300 s dehumidification, 300–600 s regeneration).

the average DCOPs were raised by 6.9 % and 12.3 %. At 100°C , the performance gap between the two hybrid wheels and silica gel wheel reached a peak (26.2 % and 7.6 % higher MRR and DCOP for S1, 20.2 % and 12.2 % for S2). Comparing to the cool&humid condition, the performance enhancement was more noticeable owing to more water vapor the process air carried to be adsorbed. The MRRs and DCOPs of silica gel wheel with $t_{\text{cyc}} = 240$ s is also presented in Fig. 14. The more frequent regeneration improved the moisture remove of silica gel wheel indeed, but with a significant disadvantage in DCOP. The MRRs of all the wheels with the optimal t_{cyc} were very close at $90\text{--}100^{\circ}\text{C}$ regeneration, and the hybrids wheels had at least 0.15 higher DCOP.

The outlet air humidity change over time under 600 s cycling time and the base conditions in Fig. 15 suggests that the hybrid desiccant wheels not only had a rapid desorption stage but also a rapid adsorption stage. According to the space-time variation map of desiccant water uptake along the channel shown in Fig. 16, the rapid adsorption stage ended when the hydrophilic desiccant meets saturation, while the rapid desorption stage ended after the complete desorption of hydrophobic and moderate desiccants. Additionally, the front section of the desiccants in hybrid desiccant wheels S1 and S2 lacked participation in cycling. Further improved configurations should be put forward in the future, such as reducing the wheel thickness while maintaining the same performance by removing the part of desiccants that do not work efficiently in adsorption/desorption cycling, or by rationally designing the

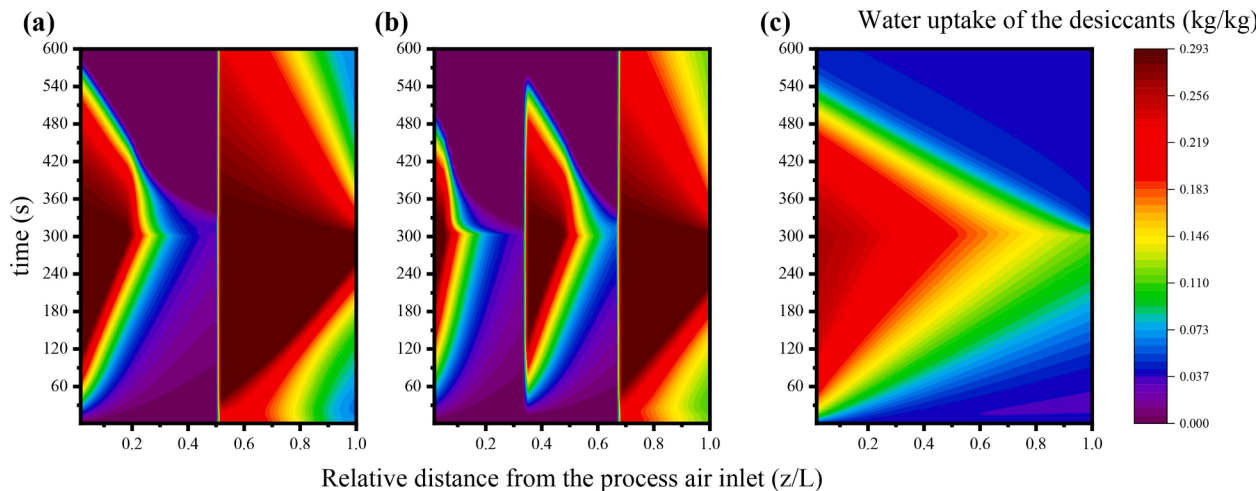


Fig. 16. Water uptake change at 80°C and 600 s cycle time under hot&humid condition.

adsorption time and desorption time to avoid the early end of rapid adsorption/desorption stages.

Section 2.1&2.2 specify the performance advantages of the hybrid wheels. Compared to the silica gel wheel, the *MRRs* and *DCOPs* of S1 and S2 were improved simultaneously under the same long cycle time with the regeneration temperature reaching the critical value. The continuously stable humidity of the output air brought by the staged adsorption may be beneficial. Despite the higher *MRRs* of silica gel wheel at its best performance, the *DCOPs* were unsatisfactory. Meanwhile the frequent regeneration needed for silica gel wheel would consume more mechanical energy to rotate the wheel and bring noise. Moreover, there is plenty of room for the improvement of the hybrid configurations investigated.

5. Conclusion

In this study, the air dehumidification performance of two counter flow type hybrid desiccant wheels with hypothetical type-S isotherm desiccants were analyzed and compared with a silica gel wheel through a one-dimensional transient heat and mass transfer model. Two kinds of hybrid configurations S1 and S2 were considered. The concept proposed in this study may stimulate the interest of those desiccants regarded as moderate and hydrophobic, and may be used in many adsorptive related field (e.g., adsorption refrigeration, air separation by adsorption, etc.).

The main conclusions can be summarized as follows:

- 1) Long cycling time and regeneration temperature exceeding the critical value are needs for the superior performance advantages of the studied hybrid desiccant wheel configurations S1 and S2.
- 2) Compared to the silica gel wheel, the average *MRR* of S1 and S2 increases by 7.2 % and 4.8 %, respectively, while the average *DCOP* by 5.6 % and 12.4 % when the cycling time is 600 s/r and the regeneration temperature varies from 70 °C to 100 °C under cool & humid condition. The average *MRR* increases by 19.4 % and 14.7 %, respectively, while the average *DCOP* by 6.9 % and 12.3 % when the rotation speed is 6 r/h and the regeneration temperature varies from 80 °C to 120 °C under hot& humid condition.
- 3) The outlet air humidity during dehumidification is more stable for S1 and S2, which means they are suitable for places demanding high humidity control accuracy.
- 4) There is much room for improvement of hybrid desiccant wheels with type-S isotherm desiccants. Such as reducing the length or changing the isotherm of hydrophilic desiccant to enhance the regeneration efficiency, or matching the hybrid mode with the

operation conditions to avoid the slow desorption/adsorption stage. More configurations should be considered in the future.

- 5) Since the critical regeneration temperature is relatively high, the hybrid desiccant wheel proposed in this study can be used for the industrial field where sufficient waste heat and waste heat can be provided.

Declaration of Competing Interest

The authors declare that they have no known competing financial interests or personal relationships that could have appeared to influence the work reported in this paper.

Data availability

Data will be made available on request.

Acknowledgement

This work was supported by the Tongji University [Project name: The variation characterization of the heat and moisture load in Low-carbon building and its air conditioning strategies for healthy environment].

References

- [1] T.S. Ge, F. Ziegler, R.Z. Wang, A mathematical model for predicting the performance of a compound desiccant wheel (a model of compound desiccant wheel), *Appl. Therm. Eng.* 30 (8-9) (2010) 1005–1015.
- [2] J.A. Shamim, W.-L. Hsu, S. Paul, L. Yu, H. Daiguji, *Renew. Sustain. Energy Rev.* 137 (2021) 110456, <https://doi.org/10.1016/j.rser.2020.110456>.
- [3] Prabakaran and Chua, *Advances in desiccant dehumidification*, Springer International Publishing, 2021.
- [4] P. N. A., H. R. S. and H. R. H. Gb670638a. (1952.04.23). Patent 1949-1-12, Issued 1952.04.23.
- [5] T.S. Ge, Y.J. Dai, R.Z. Wang, Y. Li, Experimental investigation on a one-rotor two-stage rotary desiccant cooling system, *Energy* 33 (12) (2008) 1807–1815.
- [6] T.S. Ge, Y. Li, R.Z. Wang, Y.J. Dai, Experimental study on a two-stage rotary desiccant cooling system, *Int. J. Refrig.* 32 (3) (2009) 498–508.
- [7] J. Jeong, S. Yamaguchi, K. Saito, S. Kawai, Performance analysis of four-partition desiccant wheel and hybrid dehumidification air-conditioning system, *Int. J. Refrigeration* 33 (3) (2010) 496–509.
- [8] R. Narayanan, W.Y. Saman, S.D. White, A non-adiabatic desiccant wheel: Modeling and experimental validation, *Applied Thermal Eng.* 61 (2) (2013) 178–185.
- [9] X. Zhou, M. Goldsworthy, A. Sproul, *Appl. Energy* 224 (2018) 382–397.
- [10] J.D. Chung, D.-Y. Lee, Effect of desiccant isotherm on the performance of desiccant wheel, *Int. J. Refrig.* 32 (4) (2009) 720–726.
- [11] M.H. Ahmed, N.M. Kattab, M. Fouad, Evaluation and optimization of solar desiccant wheel performance, *Renew. Energy* 30 (3) (2005) 305–325.
- [12] Bhabhor and Jani. Performance analysis of desiccant dehumidifier with different channel geometry using CFD. *JOURNAL OF BUILDING ENGINEERING* (2021). 44: 103021. DOI <https://doi.org/10.1016/j.jobe.2021.103021>.

- [13] R. Narayanan, W.Y. Saman, S.D. White, M. Goldsworthy, Comparative study of different desiccant wheel designs, *Appl. Therm. Eng.* 31 (10) (2011) 1613–1620.
- [14] X. Zheng, T.S. Ge, R.Z. Wang, *Energy* 74 (2014) 280–294.
- [15] L. Yadav, A. Yadav, Effect of desiccant isotherm on the performance of a desiccant wheel at different operating conditions, *HEAT TRANSFER-ASIAN RESEARCH* 46 (6) (2017) 623–646.
- [16] FENG. Performance of desiccant wheel affected by isotherm. In *Proceedings of the 11th IIR Gustav Lorentzen Conference on Natural Refrigerants* (Hangzhou, China, 2014).
- [17] M. Sultan, T. Miyazaki, S. Koyama, *Renew. Energy* 121 (2018) 441–450.
- [18] Novosel., Advances in desiccant technologies, *Energy Eng.* 93 (1) (1996) 6–19.
- [19] C.E.L. Nóbrega, N.C.L. Brum, Influence of isotherm shape over desiccant cooling cycle performance, *Heat Transfer Eng.* 30 (4) (2009) 302–308.
- [20] T. Kohler, M. Hinze, K. Müller, W. Schwieger, *Energy* 135 (2017) 227–236.
- [21] M.J. Goldsworthy, Measurements of water vapour sorption isotherms for RD silica gel, AQSOA-Z01, AQSOA-Z02, AQSOA-Z05 and CECA zeolite 3A, *Microporous Mesoporous Materials* 196 (2014) 59–67.
- [22] S. Inagaki, Y. Fukushima, K. Kuroda, K. Kuroda, Adsorption isotherm of water vapor and its large hysteresis on highly ordered mesoporous silica, *J. Colloid Interface Sci.* 180 (2) (1996) 623–624.
- [23] A. Khutia, H.U. Rammelberg, T. Schmidt, S. Henninger, C. Janiak, Water sorption cycle measurements on functionalized MIL-101Cr for heat transformation application, *Chem., Materials* 25 (5) (2013) 790–798.
- [24] J.S. Oh, W.G. Shim, J.W. Lee, J.H. Kim, H. Moon, G. Seo, Adsorption Equilibrium of Water Vapor on Mesoporous Materials, *J. Chem. Eng. Data* 48 (6) (2003) 1458–1462.
- [25] G. Li, K. Kaneko, F. Okino, H. Touhara, R. Ishikawa, M. Kanda, Adsorption behavior of polar-molecules in fluorinated micropores, *J. Colloid Interface Science* 172 (2) (1995) 539–540.
- [26] Y. Hanzawa, K. Kaneko, Lack of a predominant adsorption of water vapor on carbon mesopores, *Langmuir* 13 (22) (1997) 5802–5804.
- [27] Burhan, Chen, and Shahzad. Parametric analysis of a universal isotherm model to tailor characteristics of solid desiccants for dehumidification. *FRONTIERS IN ENERGY RESEARCH* (2022). 10. DOI <https://doi.org/10.3389/fenrg.2022.869807>.
- [28] Chen, Li, and Zhang. Reticular access to highly porous acs-MOFs with rigid trigonal prismatic linkers for water sorption. *JOURNAL OF THE AMERICAN CHEMICAL SOCIETY* (2019). 141(7): 2900–2905. DOI <https://doi.org/10.1021/jacs.8b13710>.
- [29] M.P. Silva, A.M. Ribeiro, C.G. Silva, G. Narin, I.B.R. Nogueira, U.-H. Lee, J.L. Faria, J.M. Loureiro, J.-S. Chang, A.E. Rodrigues, A. Ferreira, Water vapor harvesting by a (P)TSA process with MIL-125(Ti)_{NH2} as adsorbent, *Sep. Purif. Technol.* 237 (2020) 116336.
- [30] H. Furukawa, F. Gándara, Y.-B. Zhang, J. Jiang, W.L. Queen, M.R. Hudson, O. M. Yaghi, *J. Am. Chem. Soc.* 136 (11) (2014) 4369–4381.
- [31] Ž. Knez, Z. Novak, Adsorption of water vapor on silica, alumina, and their mixed oxide aerogels, *J. Chem. Eng. Data* 46 (4) (2001) 858–860.
- [32] Muthu, Talukdar, and Jain. Performance enhancement of rotary desiccant wheel by innovative designs of multiple desiccant layers. In *5th International and 41st National Conference on Fluid Mechanics and Fluid Power*, 2017.
- [33] T.S. Ge, Y. Li, R.Z. Wang, Y.J. Dai, *Renew. Sustain. Energy Rev.* 12 (6) (2008) 1485–1528.
- [34] D.B. Jani, M. Mishra, P.K. Sahoo, *Renewable Sustainable Energy Reviews* 60 (2016) 1451–1469.
- [35] DeWitt Incropera, Bergman., *Fundamentals of heat and mass transfer*, Wiley, 2007.
- [36] ajumdar. Heat and mass transfer in composite desiccant pore structures for dehumidification. *SOLAR ENERGY* (1998). 1: 1–10. DOI [https://doi.org/10.1016/S0038-092X\(97\)00080-7](https://doi.org/10.1016/S0038-092X(97)00080-7).
- [37] L.Z. Zhang, J.L. Niu, Performance comparisons of desiccant wheels for air dehumidification and enthalpy recovery, *Appl. Therm. Eng.* 22 (12) (2002) 1347–1367.
- [38] Cheng, Peters, and Kuipers. Numerical modelling of flow and coupled mass and heat transfer in an adsorption process. *CHEMICAL ENGINEERING SCIENCE* (2016) 413–425. DOI <https://doi.org/10.1016/j.ces.2016.06.036>.
- [39] Brillhar., Evaluation of desiccant rotor matrices using an advanced fixed-bed test system, University of Illinois at Chicago, Thesis, 1997 <https://hdl.handle.net/10027/17329>.